Surface plasmons on n-type semiconductors: Influence of depletion and accumulation layers

D. H. Ehlers* and D. L. Mills
Department of Physics, University of California, Irvine, California 92715
(Received 10 November 1986)

We study surface plasmons on n-type semiconductors, for realistic and nonuniform free-carrier density profiles, and through use of a nonlocal description of the response of the electrons. A random-phase-approximation description is employed, with the irreducible particle-hole propagator calculated from wave functions generated by a self-consistent potential. For the case of n-type GaAs, we present quantitative studies of the dispersion of surface plasmons, Landau damping of these modes, and frequency shifts induced by a depletion or accumulation layer. The emphasis is on the range of wave vectors probed in near-specular electron-energy-loss studies.

I. INTRODUCTION

One consequence of introducing free carriers into semiconductors is the appearance of collective excitations at the surface known as surface plasmons. The simplest theoretical description of these modes is within a macroscopic theory which regards the material as a semi-infinite dielectric,[1] with frequency-dependent dielectric constant $\epsilon(\omega)$. With retardation ignored, the frequency ω_s of the surface plasmon is determined through the relation $\epsilon(\omega_s)=-1$. If ω_p is the plasma frequency of the free carriers,[2] and ϵ the dielectric constant, then $\epsilon(\omega)=\epsilon-\omega_p^2/\omega^2$, and $\omega_s=\omega_p/(1+\epsilon)^{1/2}$. If the background dielectric constant ϵ is itself frequency dependent, possibly by virtue of infrared active transverse optical (TO) phonons in the material, there may be two or more solutions of the equation $\epsilon(\omega)=-1$, and the surface modes are viewed as coupled modes of the conduction electrons, and optical-phonon modes.

Surface plasmons, or coupled surface-plasmon–phonon modes appear as loss peaks in electron-energy-loss studies of semiconductor surfaces, in the near-specular geometry.[3] This particular form of spectroscopy is potentially a most interesting means of probing surface plasmons. The reason is that the range of wave vectors explored ranges from 0, to the order of 10^6 cm^{-1}. Near semiconductor surfaces, or at the interface between a semiconductor and another material, substantial variations in the free-carrier profile occur on the scale of one hundred, to a few hundred angstroms. If l is the thickness of this region, then the electron-energy-loss method explores the wave-vector regime $q_{\parallel}l\cong 1$, where the nonuniform free-carrier density profile can be expected to influence the dispersion relation and amplitude of the surface plasmons importantly. We thus have a means of probing the dynamics of a spatially nonuniform electron gas, and also extracting information on the nature of free carriers very close to the surface of semiconducting materials.

The spatial variation of the free-carrier density is influenced by a number of factors. For an ideal surface in vacuum, the occupied conducting states lie several volts below the vacuum level. The resulting potential barrier requires the wave function to have very small amplitude on the surface; to a very good approximation the wave functions may be said to vanish there, when viewed on the length scale of a few hundred angstroms. This boundary condition on all wave functions suppresses the free-carrier charge density near the surface, over a length scale controlled by the average de Broglie wavelength of the electrons. We may view this as a kinematical effect, ignored in Thomas-Fermi descriptions of the free carrier profiles.[4] Also, a semiconducting surface or interface can also carry a net charge, by virtue of traps, defects or adsorbates present there. This produces band bending, and an accumulation (depletion) layer if the net surface charge is positive (negative). In a recent paper,[5] we have presented self-consistent calculations of the spatial variation of the conduction-electron density near the surface of a n-type GaAs, for the case where the surface is charge neutral, or bears net positive or negative charge. The model smears the charge density produced by ionized donors in the bulk into a jellium background, and introduces the effect of the surface charge through a uniform electric field emanating from the surface.

Given the free-carrier density profile, optimally generated through a self-consistent calculation such as that just described, the next task is to evaluate the dispersion relation and other properties of the surface plasmons. There is a considerable amount of literature on an approach which proceeds as follows. The material is assumed to be described by a dielectric constant which depends not only on the frequency ω, but position z from the surface. Thus if $\mathbf{D}(\mathbf{x},\omega)$ and $\mathbf{E}(\mathbf{x},\omega)$ are the displacement and electric fields and $\epsilon(z,\omega)$ the dielectric function, we have $\mathbf{D}(\mathbf{x},\omega)=\epsilon(z,\omega)\mathbf{E}(\mathbf{x},\omega)$. If $r(z)=n(z)/n_0$, with $n(z)$ the free carrier at z and n_0 the carrier density in the bulk, then one supposes that $\epsilon(z,\omega)=\epsilon-r(z)\omega_p^2/\omega^2$, an approximation surely appropriate to situations where the carrier density varies slowly in space. With this relation between $\mathbf{D}$ and $\mathbf{E}$, one may analyze the solution to Maxwell's equations to determine the free-carrier response.

While the above-mentioned local dielectric response description has been applied to semiconductor surfaces where an accumulation or depletion layer is present,[6,7] in fact the criterion for the validity of the approach is not met in these systems. The difficulty is that the thickness l of the nonuniform layer is controlled by a combination of the de Broglie wavelength of the electrons, and the Debye

(or Thomas-Fermi) screening length, both of which have similar magnitude in typical cases.[8] Under these circumstances, the current density and consequently $\mathbf{D}(\mathbf{x},\omega)$ is not proportional to $\mathbf{E}(\mathbf{x},\omega)$ evaluated at the same point, but instead is an average over values of $\mathbf{E}(\mathbf{x},\omega)$ throughout a volume whose linear dimension is the order of l. A nonlocal description of the response of the electron gas must be employed.

The purpose of this paper is to present a full nonlocal description of surface plasmons at the surface of a doped semiconductor, with application to n-type GaAs. We remark that the motivation for our investigation is the appearance of the works of Matz and Lüth[9] and Ritz and Lüth.[10] These authors explored surface plasmons on n-type GaAs and InSb, respectively, with near-specular electron-energy-loss spectroscopy. Matz and Lüth observe frequency shifts of the modes when hydrogen is chemisorbed on the surface, evidently as a consequence of depletion layer formation, while Ritz and Lüth found a strong dependence of mode intensity, position and linewidth on the wave vector transfer $q_\parallel$. This work raises the question of the quantitative relation between the charge residing on the surface, and shifts of the dispersion relation from that appropriate to the ideal surface (near which the free-carrier density profile is necessarily nonuniform, for reasons cited earlier).

We use the free-carrier wave functions generated by our earlier self-consistent calculation of the free-carrier density profile to calculate the irreducible particle-hole propagator $\chi_0(\mathbf{q}_\parallel,\omega;z,z')$ which enters the nonlocal theory. We then solve for the full response function $\chi(\mathbf{q}_\parallel,\omega;z,z')$ within an RPA description of the response of the nonuniform electron gas. Correlation and exchange effects are small for the range of densities and temperatures explored here,[5] so we ignore these both in generating the free-carrier density profile and in the nonlocal description of the dynamics of the surface regime. We note that within this approach, the force sum rule is satisfied.[11] Given $\chi(\mathbf{q}_\parallel,\omega;z,z')$, we form the loss function $P(\mathbf{q}_\parallel,\omega)$ which enters the description of the electron energy-loss process.[3,12] Through an analysis of the structure of this function, we obtain information on the dispersion relation of the surface plasmons, their width as a consequence of Landau damping, and the spatial variation of the electric fields generated by the waves. Throughout the discussion, retardation effects are ignored. These have negligible influence on electron-energy-loss spectra.

We also remark that there is an unphysical feature of the local response approach[6,7] absent from the full nonlocal approach used in this paper. The bulk plasmon frequency, in notation used here, is $\omega_p/\sqrt{\epsilon}$, and (with the possible exception of the case where a strong accumulation layer is present), the surface plasmons lie below this frequency. Then there is a particular value of z, z_0, where $\epsilon(z_0,\omega)=0$. The electric fields generated by the surface plasmon are singular at $z=z_0$, where the electron gas exhibits a strong local resonance in response to the electric fields set up by the surface plasmon.[13] Such unphysical singularities are absent in the nonlocal theory.

We note also that in the earlier literature,[7] a controversy appeared over the question of whether new surface plasmon branches can appear, in the presence of nonuniform free-carrier density profiles. Our numerical work fails to find such additional branches, even for very strong accumulation layers.[14] We do not regard our work as settling the earlier controversy, which concerned the existence of new branches only within the framework of the local dielectric response description. Also, some of these structures may exist only when retardation is included.

The outline of this paper is as follows. In Sec. II we discuss our approach, and explore properties of the basic equation. In Sec. III we discuss issues related to the numerical computations; we have found the task of achieving guaranteed convergence in the semi-infinite geometry challenging, and the discussions of numerical procedures in the earlier literature rather sparse. In Sec. IV we present and discuss our results.

II. THEORETICAL DISCUSSION

It is useful to present the results by calculating a response function which directly enters an experimental measurement. As indicated in Sec. I, the very beautiful near-specular electron energy-loss studies of n-type GaAs reported by Matz and Lüth motivate us to calculate the spectrum observed in such an experiment.

A rather general description of this experiment was provided some years ago.[12] The physical picture is the following. There are charge fluctuations within the material, and we describe these by the charge fluctuation operator $\delta\rho(\mathbf{x},t)$. Those charge fluctuations characterized by the wave vector $\mathbf{q}_\parallel$ parallel to the surface produce fluctuating electric fields outside the crystal with the spatial variation $\exp(-q_\parallel|z|)$. Thus, charge fluctuations with long wavelengths parallel to the surface produce long-ranged fields fluctuating outside which an incoming electron couples to strongly. A consequence is that the cross section for energy loss is very large, for the small angle deflections produced by such long-ranged fields.

We may describe the resulting near-specular lobe by introducing the scattering efficiency per unit frequency, $dS/d\omega$, which is the probability the electron reflects off the surface to emerge in the near specular loss lobe, with energy loss between ω and $\omega+d\omega$. This quantity may be written[15]

$$\frac{dS}{d\omega}=\frac{2e^2v_\perp^2}{\pi\hbar}|R_I|^2\int d^2q_\parallel\frac{P(q_\parallel,\omega)}{[v_\perp^2q_\parallel^2+(\omega-\mathbf{v}_\parallel\cdot\mathbf{q}_\parallel)^2]^2}\ . \quad (2.1)$$

Here, $v_\perp$ and $\mathbf{v}_\parallel$ are the components of the incident electron's velocity perpendicular and parallel to the surface, $|R_I|^2$ the probability the electron scatters elastically from the surface to emerge in the specular direction, and if the crystal lies in the upper half space $z>0$, we have

$$P(q_\parallel,\omega)=\frac{e^2}{\hbar}\int d^2x_\parallel\int_{-\infty}^{+\infty}dt\exp(i\mathbf{q}_\parallel\cdot\mathbf{x}_\parallel-i\omega t)\int_{0-}^{\infty}dz'\int_{0-}^{\infty}dz''\exp[-q_\parallel(z'+z'')]\langle\delta\rho^\dagger(\mathbf{x}_\parallel,z'';t)\delta\rho(\mathbf{0},z';0)\rangle_T\ , \quad (2.2)$$

with $\delta\rho(\mathbf{x}_\parallel,z;t)$ the charge fluctuation operator introduced earlier, with argument written slightly differently, and the angular brackets denote a statistical average of the enclosed operator over a statistical ensemble in equilibrium at temperature T.

When $q_\parallel$ is small, the crystal may be viewed as a semi-infinite dielectric with (complex) dielectric function $\epsilon(\omega)$, and the fluctuation dissipation theorem may be used to evaluate the right hand side of Eq. (2.2).[12] In this picture, one finds

$$P(q_\parallel,\omega)=[1+n(\omega)]\frac{2q_\parallel}{\pi}\mathrm{Im}\left[\frac{-1}{1+\epsilon(\omega)}\right], \tag{2.3}$$

a result we refer to later. In Eq. (2.3), $n(\omega)=[\exp(\beta\hbar\omega)-1]^{-1}$ is the Bose-Einstein function. Surface plasmons contribute as a consequence of the resonance on the right-hand side of Eq. (2.3) at $\epsilon(\omega)=-1$.

To return to the general discussion, we Fourier transform the spatial variables parallel to the surface by writing

$$\delta\rho(\mathbf{x}_\parallel,z;t)=\frac{1}{\sqrt{A}}\sum_{\mathbf{q}_\parallel}e^{i\mathbf{q}_\parallel\cdot\mathbf{x}_\parallel}\delta\rho(\mathbf{q}_\parallel,z;t), \tag{2.4}$$

with A a quantization area parallel to the surface. We then have

$$P(q_\parallel,\omega)=\frac{e^2}{\hbar}\int_{-\infty}^{+\infty}dt\,e^{-i\omega t}\int_{0-}^{\infty}dz'\int_{0-}^{\infty}dz''\,e^{-q_\parallel(z'+z'')}\langle\delta\rho^\dagger(\mathbf{q}_\parallel,z';t)\delta\rho(\mathbf{q}_\parallel,z'';0)\rangle_T . \tag{2.5}$$

In the above expressions, the operator $\delta\rho(\mathbf{q}_\parallel,z;t)$ describes the *total* charge fluctuation amplitude in the crystal.[12] In our example of a doped semiconductor, we have the fluctuations $\delta\rho_e(\mathbf{q}_\parallel,z;t)$ associated with electrons in the conduction band, and it is these we wish to study microscopically. There are additional contributions from sources such as interband transitions. We incorporate these into a background dielectric constant ϵ, assumed described adequately by optical measurements at the long wavelengths and frequency range of interest here.

The following argument links the total charge fluctuation amplitude $\delta\rho(\mathbf{q}_\parallel,z;t)$ to that associated with only the conduction electrons. Consider the electrons to be imbedded in a semi-infinite dielectric, with dielectric constant ϵ, and calculate the potential outside the crystal. With the crystal in the half space $z>0$, this is given by

$$\delta\Phi(\mathbf{x},t)=\Phi^<\exp(i\mathbf{q}_\parallel\cdot\mathbf{x}_\parallel)\exp(q_\parallel z),$$

with

$$\Phi^<=\frac{4\pi e}{q_\parallel(1+\epsilon)}\int_{0-}^{\infty}dz'\,e^{-q_\parallel z'}\delta\rho_e(\mathbf{q}_\parallel,z';t) . \tag{2.6a}$$

In terms of the total charge fluctuation amplitude $\delta\rho(\mathbf{q}_\parallel,z';t)$ we have

$$\Phi^<=\frac{2\pi e}{q_\parallel}\int_{0-}^{\infty}dz'\,e^{-q_\parallel z'}\delta\rho(\mathbf{q}_\parallel,z';t), \tag{2.6b}$$

so for the purposes of calculating the electron energy-loss cross section, we may replace $\delta\rho(\mathbf{q}_\parallel,z;t)$ by $[2/(1+\epsilon)]\delta\rho_e(\mathbf{q}_\parallel,z;t)$. Thus, we write

$$P(\mathbf{q}_\parallel,\omega)=\frac{4}{|1+\epsilon|^2}P_e(\mathbf{q}_\parallel,\omega), \tag{2.7}$$

where $P_e(\mathbf{q}_\parallel,\omega)$ has the form given in Eq. (2.5), with $\delta\rho(\mathbf{q}_\parallel,z;t)$ replaced by $\delta\rho_e(\mathbf{q}_\parallel,z;t)$.

In our treatment of the dynamics of the electron gas, we shall generate the equation satisfied by the density-density correlation function

$$\chi(\mathbf{q}_\parallel,t;z,z')=\frac{i\theta(t)}{\hbar}\langle[\delta\rho_e^\dagger(\mathbf{q}_\parallel,z;t),\delta\rho_e(\mathbf{q}_\parallel,z';0)]\rangle_T , \tag{2.8}$$

which we write in the form

$$\chi(\mathbf{q}_\parallel,t;z,z')=\int_{-\infty}^{+\infty}\frac{d\omega}{2\pi}\chi(\mathbf{q}_\parallel,\omega;z,z')e^{-i\omega t} . \tag{2.9}$$

After some standard algebra, we find

$$P_e(\mathbf{q}_\parallel,\omega)=2e^2[1+n(\omega)]\times\int_{0-}^{\infty}dz\int_{0-}^{\infty}dz'\,e^{-q_\parallel(z+z')}\mathrm{Im}[\chi(\mathbf{q}_\parallel,\omega;z,z')] . \tag{2.10}$$

We next turn to the description of the equation that must be solved to obtain $\chi(\mathbf{q}_\parallel,\omega;z,z')$. As remarked above, we generate this through use of the RPA. While the derivation is standard, we shall summarize the structure of the theory, so the various definitions are clear.

As remarked in Sec. I, our basic model is as follows. We consider n-type semiconductors with electrons in a parabolic band of effective mass m^*, and the background dielectric constant is ϵ. The ionized donors are smeared out into a uniform positive background, which just cancels the charge density generated by the free carriers in the bulk. A thin sheet of charge, with charge density $-Q_s$ is placed on the surface. This represents the trapped charges on the surface responsible for the accumulation or depletion layer. The number Q_s thus represents the conduction electron charge displaced by the presence of the surface charge, with a conduction electron deficit (depletion layer) corresponding to positive Q_s. For this model, the conduction electron wave function has the form

$$\phi_{\mathbf{k}_\parallel i}(\mathbf{x})=\frac{e^{i\mathbf{k}_\parallel\cdot\mathbf{x}_\parallel}}{(A)^{1/2}}\psi_i(z), \tag{2.11}$$

and the energy eigenvalue is $E_{\mathbf{k}_\parallel i}=(\hbar^2k_\parallel^2/2m^*)+\varepsilon_i$. The conduction electrons reside in states which lie several electron volts below the vacuum level, in the systems of interest. The depletion or accumulation layer has a thickness of a few hundred angstroms, and on this length scale we may ignore the small tail of the wave function which extends into the vacuum. We thus impose the boundary condition

$$\psi_i(0)=0 \ . \tag{2.12}$$

In our preceding paper,[5] we discussed a means of efficiently generating the function $\psi_i(z)$ from a self-consistent potential, and we carried out explicit calculations for the surfaces of n-type GaAs. The procedure, introduced by Baraff and Appelbaum,[16] fits a model potential of the Morse form to the self-consistent potential, taken to be the Hartree potential; exchange and correlation effects were estimated to be quite small, for the case of interest to us. As is the case in the present paper, our previous calculations were carried out for room temperature, with no approximations introduced to describe the statistical mechanics of the free carriers.

The virtue of the method, exploited further here, is that a simple series expression is in hand for the eigenfunctions $\psi_i(z)$, so these need not be generated by numerically solving a Schrödinger equation. For continuum states with $\varepsilon_i > 0$, these functions may be written

$$\psi_i(z)=C(i)\mathrm{Im}[e^{i\eta(i)}\xi_i(z)] \ , \tag{2.13}$$

where $C(i)$ is a normalization constant, and $\xi_i(z)$ has the form

$$\xi_i(z)=\exp(ik_\perp^{(i)}z)\sum_{m=0}^{\infty} b_m(i)e^{-m\mu z} \ . \tag{2.14}$$

The bound states generated when an accumulation layer is present are simply proportional to $\xi_i(z)$, with $k_\perp^{(i)}$ imaginary. The phase shift $\eta(i)$ and expansion coefficient $b_m(i)$ are determined as described earlier,[5,16] while μ is a parameter contained in the Morse potential.

We now use the above basic states as a representation, and derive the equation satisfied by the response function introduced in Eq. (2.8), by invoking the random-phase approximation. Only the final result is quoted, since the procedure is straightforward, and save for details, has been discussed by others in a number of contexts. The result is

$$\begin{aligned}\chi(\mathbf{q}_\parallel,\omega;z,z')=&\chi_0(\mathbf{q}_\parallel,\omega;z,z')\\ &-\int_0^\infty dz''\int_0^\infty dz'''\,\chi_0(\mathbf{q}_\parallel,\omega;z,z'')\\ &\times v(\mathbf{q}_\parallel;z'',z''')\\ &\times\chi(\mathbf{q}_\parallel,\omega;z''',z') \ ,\end{aligned} \tag{2.15}$$

where $v(\mathbf{q}_\parallel;z'',z''')$ is a suitably defined Fourier transform of the electron-electron interaction, and $\chi_0(\mathbf{q}_\parallel,\omega;z,z'')$ is the irreducible particle-hole propagator, given in this instance by, with an explicit factor of two for spin,

$$\begin{aligned}\chi_0(\mathbf{q}_\parallel,\omega;z,z')=&\frac{2}{A}\sum_{\mathbf{k}_\parallel}\sum_{i,j}\frac{[f(\mathbf{k}_\parallel,i)-f(\mathbf{k}_\parallel+\mathbf{q}_\parallel,j)]}{\hbar\omega+i\delta+E_{\mathbf{k}_\parallel+\mathbf{q}_\parallel,j}-E_{\mathbf{k}_\parallel i}}\\ &\times\psi_i^*(z)\psi_i(z')\psi_j(z)\psi_j^*(z') \ .\end{aligned} \tag{2.16}$$

Here,

$$f(\mathbf{k}_\parallel,i)=\{\exp[\beta(E_{\mathbf{k}_\parallel i}-\mu)]+1\}^{-1} \ ,$$

with $\beta=1/k_BT$, is the Fermi-Dirac function. In our numerical calculations, we do not work directly with the form in Eq. (2.16), but instead rearrange the right-hand side following the approach of Zangwill and Soven.[17] We discuss this procedure, as it applies to our case, later in Sec. III.

Our conduction electrons are imbedded in a semi-infinite dielectric with dielectric constant ϵ. Thus, when two electrons are placed within the material and close to the surface, one of these interacts with the second not only by means of the direct electron-electron interaction, but it also senses the image charge of the second. Let the coordinates of the first be $\mathbf{x}=(\mathbf{x}_\parallel,z)$ and the second be $\mathbf{x}'=(\mathbf{x}'_\parallel,z')$ and let $\boldsymbol{\rho}_\parallel=\mathbf{x}_\parallel-\mathbf{x}'_\parallel$. Then the electron-electron interaction $V(\mathbf{x},\mathbf{x}')$ has the form

$$\begin{aligned}V(\mathbf{x},\mathbf{x}')=\frac{e^2}{\epsilon}\Bigg[&\frac{1}{|\boldsymbol{\rho}_\parallel+\hat{\mathbf{z}}(z-z')|}\\ &+\left[\frac{\epsilon-1}{\epsilon+1}\right]\frac{1}{|\boldsymbol{\rho}_\parallel+\hat{\mathbf{z}}(z+z')|}\Bigg] \ ,\end{aligned} \tag{2.17}$$

and the definition of $v(\mathbf{q}_\parallel;z,z')$ in Eq. (2.15) is

$$v(\mathbf{q}_\parallel;z,z')=\int d^2\rho_\parallel\, e^{-i\mathbf{q}_\parallel\cdot\boldsymbol{\rho}_\parallel}V(\mathbf{x},\mathbf{x}') \ , \tag{2.18}$$

so we have

$$v(\mathbf{q}_\parallel;z,z')=\frac{2\pi e^2}{\epsilon q_\parallel}\left[e^{-q_\parallel|z-z'|}+\left[\frac{\epsilon-1}{\epsilon+1}\right]e^{-q_\parallel(z+z')}\right] \ . \tag{2.19}$$

The effect of the image charges is to increase the repulsive interaction between the electron pair, when they are close to the surface, so long as $\epsilon > 1$.

In general, to deduce information from Eq. (2.15), one must proceed to its solution by numerical methods (Secs. III and IV). First however, for the discussion of long-wavelength surface plasmons, our interest lies in the limit $\mathbf{q}_\parallel\to\mathbf{0}$, with the frequency ω held finite. For this case, and ω sufficiently large, it is possible to extract the structure of the solution by analytic methods. This is done in the Appendix, where it is demonstrated that

$$\begin{aligned}\lim_{\mathbf{q}_\parallel\to 0}\int_0^\infty dz\,\chi(q_\parallel,\omega;z,z')e^{-q_\parallel z}&\\ =\frac{-q_\parallel^2}{m^*\omega^2}\frac{n(z')}{1-\dfrac{4\pi n(\infty)e^2}{m^*(\epsilon+1)}\dfrac{1}{\omega^2}}& \ ,\end{aligned} \tag{2.20}$$

with $n(\infty)\equiv n_0$ the bulk free-carrier concentration in the material. For the purposes of the proof, in the Appendix we have included the correlation and exchange contributions to the effective electron-electron interaction, in the manner used commonly in extensions of density-functional theory to the analysis of response functions at

finite frequency.

The result in Eq. (2.20), derived from the generalization of Eq. (2.15) just described, has a number of implications. If we multiply each side by $\exp(-q_\parallel z')$, integrate on z' from zero to infinity, note that as $q_\parallel \to 0$,

$$\int_0^\infty dz' e^{-q_\parallel z'} n(z') \cong \frac{1}{q_\parallel} n_0 . \tag{2.21}$$

Then use Eq. (2.10), we have, with $\omega_p^2 = 4\pi n(\infty) e^2/m^*$ the plasma frequency,

$$\lim_{q_\parallel \to 0} P_e(q_\parallel,\omega) = -\frac{q_\parallel}{2\pi}[1+n(\omega)]\frac{\omega_p^2}{\omega^2} \times \mathrm{Im}\left[1\Big/1-\frac{1}{(\epsilon+1)}\frac{\omega_p^2}{\omega^2}\right], \tag{2.22}$$

where we assume implicitly that ω is replaced by $\omega+i\delta$ and $n(\omega)$ again is the Bose-Einstein function. Now ϵ is the background dielectric constant, assumed real, and let $\epsilon_T(\omega)=\epsilon-\omega_p^2/\omega^2$ be the total dielectric constant, including the free-carrier contribution. Then

$$\mathrm{Im}\left[\frac{\omega_p^2}{\omega^2}\left[-1\Big/1-\frac{1}{(\epsilon+1)}\frac{\omega_p^2}{\omega^2}\right]\right] = (\epsilon+1)\mathrm{Im}\left[\frac{\epsilon_T(\omega)-\epsilon}{\epsilon_T(\omega)+1}\right]$$
$$= (\epsilon+1)\mathrm{Im}(1) + (\epsilon+1)^2 \mathrm{Im}\left[\frac{-1}{1+\epsilon_T(\omega)}\right], \tag{2.23}$$

so that

$$\lim_{q_\parallel \to 0} P_e(q_\parallel,\omega) = \frac{q_\parallel}{2\pi}[1+n(\omega)](1+\epsilon)^2 \mathrm{Im}\left[\frac{-1}{1+\epsilon_T(\omega)}\right]. \tag{2.24}$$

When the relation between $P_e(q_\parallel,\omega)$ and $P(q_\parallel\omega)$ given in Eq. (2.7) is noted, we have

$$\lim_{q_\parallel \to 0} P(q_\parallel,\omega) = \frac{2q_\parallel}{\pi}[1+n(\omega)]\mathrm{Im}\left[\frac{-1}{1+\epsilon_T(\omega)}\right], \tag{2.25}$$

the result derived some years ago from dielectric theory.[12]

Thus, we show that in the limit described here and in the Appendix [note the remarks between Eq. (A3) and Eq. (A4)], the RPA equation for the dynamic response function, supplemented by exchange and correlation if desired, reproduces the result obtained from dielectric theory. As remarked in the Appendix, it is essential to include the image terms in the effective electron-electron interaction [Eqs. (2.17) and (2.19)] to obtain this result. The image effects are thus crucial as soon as one abandons the simple jellium model with background dielectric constant of unity, studied so extensively in the literature on metal surfaces.[18]

The proof also establishes that as $q_\parallel \to 0$, the only mode which contributes to $P(q_\parallel,\omega)$ to leading order in $q_\parallel$, is the surface plasmon of macroscopic theory. That this is so is independent of the charge profile of the free carriers. We have also made no assumption about the distribution of charge in the jellium background, except that it is uniform in the bulk of the material so the electron density $n(z)$ approaches the value $n(\infty)$ as $z \to \infty$. Thus, it applies to the model examined by Equiluz and Campbell,[19] who studied the dynamics of a thin overlayer on a free-electron metal, by adding to jellium film a thin overlayer modeled as another jellium film whose background charge density differs from that of the substrate.

The proof does not rule out the existence of other modes in the limit $q_\parallel \to 0$, but it does require their oscillator strength to be smaller than that of the principal mode by at least one factor of $q_\parallel$. If l is the thickness of the transition region between the surface and bulk, then the oscillator strength of additional modes will be smaller than that of the principal mode by at least one factor of $q_\parallel l$. In this sense all other modes which exist in the limit $q_\parallel \to 0$ must have the character of multipole modes, possibly similar to those which appear in the hydrodynamic model of Eguiluz and Quinn.[14]

This discussion raises the question, in our view, of whether such modes will emerge within any less schematic theory of collective excitations in the surface. For $q_\parallel l \ll 1$, their oscillator strength must be small, and the modes difficult to detect, by an external probe. As $q_\parallel l$ increases, so will the Landau damping overlooked in both local dielectric response and hydrodynamic models. When $q_\parallel l \sim 1$, our calculations show this damping to be severe for the principal mode, and similar conclusions ought to apply to the multipole modes. We note that Equiluz and Campbell[19] searched for, and failed to find, additional modes in their fully microscopic theory of a dense overlayer on a less dense substrate. Here we fail to find evidence for such modes also, even for very strong accumulation layers, as we discuss in Sec. IV. The reasoning in this and the preceding paragraph provides the explanation, in our view.

The point is also illustrated by the model considered by Eguiluz and Campbell, viewed entirely within dielectric theory. The relevant formulas are given elsewhere.[3] We have a substrate, with electron plasma frequency $\omega_p^{(b)}$, and an overlayer in the form of a film of thickness d, with plasma frequency $\omega_p^{(s)}$. Both background dielectric constants have the value unity, and we let $\omega_p^{(s)} > \omega_p^{(b)}$. There are two surface plasmon branches whose dispersion relation is easily established from existing formulas.[3] As $q_\parallel \to 0$, one mode, the principal mode, has a frequency which approaches $\omega_p^{(b)}/\sqrt{2}$. The second has frequency which approaches $\omega_p^{(s)}$ itself. As $q_\parallel \to 0$, the contribution

to $P(q_\parallel,\omega)$ from the high-frequency mode (an example of a multipole mode) is smaller than that of the principal mode by a factor of $q_\parallel d$.

This completes our discussion of general questions. We now turn to the representation we have used for $\chi_0(q_\parallel,\omega;z,z')$, and the computational procedures we have employed.

III. CALCULATIONS

In all of our calculations, and in the equations displayed below, we convert all quantities to dimensionless units. Energies and frequencies are all expressed in units of k_BT, and the numerical calculations we present are all carried out for $T=300$ K. A unit of length λ, as in our previous work,[5] is defined by writing $(\hbar^2/2m^*\lambda^2)=k_BT$, or $\lambda=(\hbar^2/2m^*k_BT)^{1/2}$. Thus, distances are measured in terms of λ, and we have for wave vectors $k_\parallel=\kappa_\parallel/\lambda$, with $\kappa_\parallel$ dimensionless. For GaAs, $m^*=0.069m_0$, the free electron mass, so at room temperature, $\lambda=46.2$ Å, and $\kappa_\parallel=1$ refers to a wave vector of 2.16×10^6 cm^{-1}.

We begin by discussing the structure of the irreducible particle-hole propagator defined in Eq. (2.16) which becomes

$$\chi_0(q_\parallel,\omega;z,z')=2\sum_{i,j}\int\frac{d^2\kappa_\parallel}{(2\pi)^2}\frac{[f(\boldsymbol{\kappa}_\parallel+\mathbf{q}_\parallel,j)-f(\boldsymbol{\kappa}_\parallel,i)]}{(E_{\boldsymbol{\kappa}_\parallel,i}-E_{\boldsymbol{\kappa}_\parallel+\mathbf{q}_\parallel,j}-\omega-i\delta)}\psi_i^*(z)\psi_i(z')\psi_j(z)\psi_j^*(z')\ . \tag{3.1}$$

In our dimensionless units, $E_{\boldsymbol{\kappa}_\parallel,i}=\kappa_\parallel^2+\kappa_i^2$, where $\kappa_i^2>0$ for continuum states, and $\kappa_i^2<0$ for bound states. Thus, the Fermi-Dirac function is $f(\kappa_\parallel,i)=[\exp(\kappa_\parallel^2+\kappa_i^2-\mu)+1]^{-1}$.

We rewrite Eq. (3.1) by following Zangwill and Soven.[17] We introduce a Green's function $g(\kappa^2;z,z')$ which satisfies the differential equation

$$\left[-\frac{d^2}{dz^2}+\phi(z)-\kappa^2\right]g(\kappa^2;z,z')=\delta(z-z')\ . \tag{3.2}$$

As $z\to\infty$ with z' fixed, we have outgoing boundary conditions, while $g(\kappa^2;0z')$ vanishes. Here $\phi(z)$ is the self-consistent potential, fitted to the Morse form[5]

$$\phi(z)=\frac{V_0}{(1-\beta)}(e^{-\mu z}-\beta e^{-2\mu z})\ . \tag{3.3}$$

For a given choice of bulk carrier density, and surface charge Q_s, the numerical values for the parameters in Eq. (3.3) are determined as in our earlier paper, only here we do not include the electrostatic potential induced shift of the donor level. Typical parameters are listed in Table I. Given the Green's function just introduced, we have[17]

$$\chi_0(q_\parallel,\omega;z,z')=2\sum_i\int\frac{d^2\kappa_\parallel}{(2\pi)^2}f(\kappa_\parallel,i)[\psi_i^*(z)\psi_i(z')g(\kappa_i^2-2\boldsymbol{\kappa}_\parallel\cdot\mathbf{q}_\parallel-q_\parallel^2+\omega+i\delta;z,z')+\psi_i^*(z')\psi_i(z)g(\kappa_i^2-2\boldsymbol{\kappa}_\parallel\cdot\mathbf{q}_\parallel-\omega-i\delta;z',z)]\ . \tag{3.4}$$

This simplifies further when, as in our case, the $\psi_i(z)$'s are real. Then χ_0 is symmetric in z and z' as are the Green's functions. Their explicit form is

$$g(\kappa^2;z,z')=\frac{1}{W_\kappa}[\psi_\kappa^<(z)\psi_\kappa^>(z')\Theta(z'-z)+\psi_\kappa^<(z')\psi_\kappa^>(z)\Theta(z-z')]\ . \tag{3.5}$$

Here $\psi_\kappa^<(z)$ is that solution of the homogeneous version of the differential equation in Eq. (3.2) which obeys the boundary condition $\psi_\kappa^<(0)=0$, while $\psi_\kappa^>(z)$ obeys the outgoing boundary condition. Finally, W_κ is the Wronskian

$$W_\kappa=\left[\frac{d\psi_\kappa^<}{dz}\right]\psi_\kappa^>-\left[\frac{d\psi_\kappa^>}{dz}\right]\psi_\kappa^<\ , \tag{3.6}$$

TABLE I. For GaAs at room temperature we give the parameters V_0 (surface potential in units of k_BT) and μ^{-1} (in units of λ) for different bulk carrier concentrations and surface charges Q_s (in units of λ^{-2}).

	10^{17} cm^{-3}		3×10^{17} cm^{-3}		10^{18} cm^{-3}	
Q_s	V_0	μ^{-1}	V_0	μ^{-1}	V_0	μ^{-1}
−0.16	−4.48	2.56	−3.96	1.51	−3.70	1.04
−0.08	−2.81	2.49	−2.45	1.54	−2.43	1.05
0.00	−0.30	2.48	−0.54	1.58	−1.05	1.05
+0.08	4.94	3.39	2.10	1.91	0.59	1.04
+0.16			6.58	2.04	2.42	1.21

a quantity independent of z.

From the point of view of numerical work, the virtue of the Zangwill-Soven scheme is that one need not evaluate Eq. (3.1) directly, with its singular denominator, and also one integration less to perform. Also, for the potential given in Eq. (3.3), both $\psi_\kappa^>(z)$ and $\psi_\kappa^<(z)$ may be expressed in terms of series similar to that given in Eq. (2.14). Indeed, after replacing $\kappa_\perp^{(i)}$ by κ Eq. (2.14) reads in dimensionless units

$$\xi_\kappa(z)=e^{i\kappa z}\sum_{m=0}^{\infty} b_m(\kappa)e^{-m\mu z} \tag{3.7}$$

and the (normalized) outgoing wave is simply

$$\psi_\kappa^>(z)=C(\kappa)\xi_\kappa(z)\ . \tag{3.8}$$

Equation (2.13) for $\psi_\kappa^<(z)$, however, has to be modified for complex energies as they appear in the numerical evaluation of the Green's function, where δ is small but finite. We have

$$\psi_\kappa^<(z)=C(\kappa)\frac{1}{2i}[e^{i\eta(\kappa)}\xi_\kappa(z)-D(\kappa)e^{-i\eta(\kappa)}\xi_{-\kappa}(z)]\ , \tag{3.9a}$$

with the phase shifts now determined by

$$\tan\eta(\kappa)=-\frac{\mathrm{Im}[s(\kappa)-D(\kappa)s(-\kappa)]}{\mathrm{Re}[s(\kappa)+D(\kappa)s(-\kappa)]}\ , \tag{3.9b}$$

and

$$D(\kappa)=|s(\kappa)|/|s(-\kappa)|\ ,\quad s(\kappa)=\sum_{m=0}^{\infty} b_m(\kappa)\ . \tag{3.9c}$$

For $\kappa^2>0$ and real, $D(\kappa)=1$ and hence we recover Eq. (2.13), of course.

In the formulas above, we must always choose κ such that $\mathrm{Im}(\kappa)>0$, and then we are assured that the appropriate boundary condition is satisfied as $z\to\infty$.

When the results are assembled, and one notes $\xi_\kappa^*(\kappa)=\xi_{-\kappa^*}(z)$. The Green's function has the explicit form

$$g(\kappa^2;z,z')=\frac{1}{2i\kappa}\sum_{m,n=0}^{\infty} e^{-\mu(mz+nz')}\{e^{i\kappa(z+z')}e^{2i\eta(\kappa)}b_m(\kappa)b_n(\kappa)/D(\kappa)$$
$$-e^{i\kappa|z-z'|}[b_m(-\kappa)b_n(\kappa)\Theta(z'-z)+b_m(\kappa)b_n(-\kappa)\Theta(z-z')]\}\ . \tag{3.10}$$

It is useful to note that the Green's function obeys the relations

$$g(\kappa^2;z,z')=g(\kappa^2;z',z) \tag{3.11a}$$

and

$$g(\kappa^2=c^2-i\delta;z,z')=g^*(\kappa^2=c^2+i\delta;z,z')\ . \tag{3.11b}$$

These identities reduce the number of times one must compute the Green's functions which enter Eq. (3.4).

Note that the Green's function is independent of the normalization convention chosen for the functions $\psi_\kappa^>(z)$ and $\psi_\kappa^<(z)$. Also, when the sum on i in Eq. (3.4) is converted to an integral over the continuum as in Ref. (5), the normalization of the continuum states $\psi_i(z)$ drops out. However, when bound states are present, of course they contribute in the sum over i, and these must be explicitly normalized.

We have chosen $\mathbf{q}_\parallel$ parallel to the x direction, which leads to no loss of generality, since all quantities depend on only $|\mathbf{q}_\parallel|$. In the numerical work, it is then convenient to convert the integral on $\kappa_\parallel^{(x)}$ to one over c, where the Green's functions are written $g(c^2+i\delta;z,z')$.

Our basic numerical procedure is to discretize the variables z'' and z''' which enter Eq. (2.15), also cutting off the integration on both variables at a value z_c. The integral equation is then solved by a matrix inversion. Of course, it is essential to check convergence by varying the grid spacing for fixed z_c, and also increasing the value of z_c.

Quite clearly, examination of the various functions which enter the theory, such as the electron-electron interaction [Eq. (2.19)] shows that we cannot explore values of $q_\parallel$ so small that $q_\parallel z_c \lesssim 1$. Thus, for the semi-infinite geometry explored here, in the numerical work, we cannot achieve the limit $q_\parallel\to 0$. We have been able to obtain reliable results for $q_\parallel$ as small as 0.1 in our dimensionless units, however. One advantage of studying a finite film, as opposed to the semi-infinite geometry examined in this paper is that the integration on z'' and z''' are both bounded, so the limit $q_\parallel\to 0$ may be studied explicitly. At the time of this writing, studies of the finite film have been initiated.

Griffin and Harris[20] have derived an important sum rule which provides a useful check on the numerical calculations. In our reduced units, the sum rule reads, where P is measured in units of $(\lambda^2 k_B T)^{-1}$, and when the factor of e^2 is omitted from its definition,

$$\int_0^\infty d\omega\,\omega P(q_\parallel,\omega)=2\pi q_\parallel^2\int_0^\infty dz\, n(z)e^{-2q_\parallel z} \tag{3.12}$$

and $n(z)=\sum_i \ln(1+e^{\mu-\varepsilon_i})|\psi_i(z)|^2$ is the electron density at z, in units of λ^{-3}. In the calculations reported here, the sum rule is found to be satisfied to within roughly 1%.

We next turn to the properties of the kernel $\chi_0(q_\parallel,\omega;z,z')$. As both z and z' are moved into the bulk of the material, the kernel becomes a function of only $(z-z')$. Furthermore, the values of $\chi_0(q_\parallel,\omega;z,z')$ in the bulk should be independent of the choice of the details of the near surface region, such as surface charges. We have checked this by comparing the bulk behavior of $\chi_0(q_\parallel,\omega;z,z')$ calculated with the eigenfunctions $\psi_i(z)$ generated by the self-consistent potential, and those provided by the infinite barrier model, to find this condition

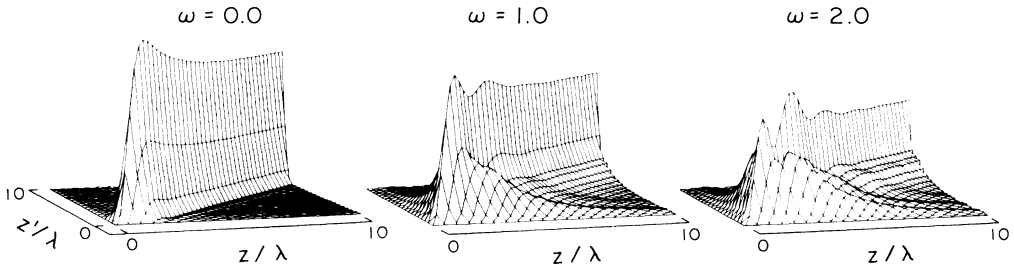

FIG. 1. For $q_{\parallel}=0.4$ and $Q_s=0$, we illustrate the dependence of $\chi_0(q_{\parallel}\omega;z,z')$ on z and z', for three values of the dimensionless frequency ω. The bulk carrier concentration is $n_0=3\times10^{17}$ cm^{-3}. Recall that $\chi_0(q_{\parallel}\omega;z,z')$ is symmetric under interchange of z and z'.

satisfied. A comparison with the χ_0 in a model with periodic boundary conditions provided a useful check on the various factors that enter the expression for $\chi_0(q_{\parallel},\omega;z,z')$, and the accuracy of the integration routines.

In Fig. 1, we plot the kernel $\chi_0(q_{\parallel},\omega;z,z')$ for a carrier concentration of 3×10^{17} cm^{-3}, $q_{\parallel}=0.4$, $Q_s=0.0$, and various values of the frequency. Except in the static limit where $\chi_0(z=z')$ mimics the density profile $n(z)$, the range of the kernel is quite large, when either z or z' lies near the surface. It is not obvious why this is so, but from these graphs one easily appreciates the need for a proper nonlocal theory, if the influence of the near surface region on the properties of surface plasmons is of interest. It is difficult to justify use of the local dielectric theory employed in the earlier literature.[6,7]

As remarked above, we must cut off the integrations on z'' and z''' in Eq. (2.15) at some value z_c, and one expects z_c must scale as $q_{\parallel}^{-1}$ to achieve convergence. We have found the choice $z_c=4/q_{\parallel}$ to be quite satisfactory, when calculating the loss function in Eq. (2.10). This simple rule was found to hold even for $q_{\parallel}$ as big as unity, where z_c is not so far from the inhomogeneous surface region; we see in Fig. (1) that the range of $\chi_0(q_{\parallel},\omega;z,z')$ can be appreciable. Perhaps the strong Landau damping causes the response of the system to be smooth and to exhibit strong spatial decay so that in the end, z_c need not be larger than given by the above rule.

Independently of the value of $q_{\parallel}$, the grid size in the z variable was taken to be $\Delta z=0.25$ in our spatial integrations. This is sufficient for proper resolution of the spatial structures near the surface. Since Δz was chosen independently of $q_{\parallel}$ (clearly this is required, since the dimensionless length λ controls the range of the spatial inhomogeneity near the surface), the size of the matrix χ_0 which must be calculated varies strongly with $q_{\parallel}$. For a typical intermediate value of $q_{\parallel}$, such as $q_{\parallel}=0.4$, we are dealing with a 40×40 matrix.

The sum over i in Eq. (3.4) includes a discrete number of bound states, if these are present, and one then includes the continuum in which the sum formally is replaced by an integration. Clearly a sufficient number of continuum states must be included in the numerical work for the charge density to be properly reproduced in the region $0<z<z_c$. No numerical oscillations must appear, as a result of inclusion of too few continuum states. Thus, if $\Delta\kappa$ is the spacing between adjacent level, we must have $\Delta\kappa z_c \lesssim \pi/2$. This means, notice, that as $q_{\parallel}$ decreases, we must also make $\Delta\kappa$ smaller. Not only does the size of the matrix one must invert increase, but at the same time the κ integration grid must be made finer.

We proceeded as follows, in all calculations reported here. For $z_c=40$, appropriate to $q_{\parallel}=0.1$, the smallest value of $q_{\parallel}$ we have considered, and $\kappa_{\max}=3.5$, we need roughly 100 continuum states. We have kept this number constant for the larger values of $q_{\parallel}$. The same value 3.5 has been chosen as the upper limit for the remaining two integrations on the components of $\boldsymbol{\kappa}_{\parallel}$, the total electron energies never exceeding $(3.5)^2k_BT$. This cutoff is large enough, so long as the Fermi energy does not lie too far above the bottom of the conduction band. As remarked earlier, the integration on κ_x is converted to an integration over c, the argument of the Green's function in $g(c^2+i\delta;z,z')$. In order to ensure numerical convergence in this step even for small $q_{\parallel}$, we take $\Delta c=\Delta\kappa_{\alpha}/2$.

Considerable care has to be taken in the choice of the "infinitesimal" quantity δ. This is kept small but finite in the numerical work. If it is too small, one encounters accuracy problems in the integration over c, and if it is too large, then results of the computation will vary with δ, in effect introducing artificial damping. We experimented with the choice of δ by noting that in the bulk of the material, one may derive a simple expression for $\mathrm{Im}[\chi_0(q_{\parallel}=0,\omega;z,z)]$. This is

$$\mathrm{Im}[\chi_0(q_{\parallel}=0,\omega;z,z)] = \int_0^{\infty}\frac{d\kappa}{4\pi^2}\ln\left[\frac{1+e^{\mu-\kappa^2}}{1+e^{\mu-\omega-\kappa^2}}\right]\frac{1}{(\omega+\kappa^2)^{1/2}}\ . \quad (3.13)$$

We found that δ has to be chosen equal to $\Delta\kappa$, here the grid width in the integration over the continuum states. In the integral over the variable c involving $g(c^2+i\delta;z,z')$, we therefore chose $\delta=\Delta c$. For small values of $q_{\parallel}$, we then reproduced results that closely match those obtained from Eq. (3.13), when z and z' are large enough for the bulk limit to be realized.

We consider our calculation of the loss function to have converged, when its accuracy was better than 2%. The frequency was scanned with a grid of width $\Delta\omega=0.025$ near the peak of the loss function, and we required the peak to be stable in position, on such a mesh. These two specifications were met with the integration and matrix

sizes controlled by the parameters given above, and, once again, the sum rule displayed in Eq. (3.12) has been checked, and found to be obeyed at the 1 % level.

With the integration procedure and matrix sizes given above, the calculation of one spectral point of the loss function for an intermediate wave vector $q_{\parallel}=0.4$ typically requires 5 sec of CPU (central processing unit) time on a Cray XMP supercomputer.

We now turn to a discussion of our results.

IV. RESULTS AND CONCLUSIONS

We present our results in terms of the dimensionless units introduced earlier. Thus, units of wave vector $q_{\parallel}$ are the inverse of the length $\lambda=(\hbar^2/2m^*k_BT)^{1/2}=46.2$ Å, for GaAs at $T=300$ K. As remarked earlier, $q_{\parallel}=1$ corresponds to a wave vector of 2.16×10^6 cm^{-1}, and the range $0\leq q_{\parallel}\lesssim 1$ corresponds to that explored in near-specular electron-energy-loss spectroscopy. Frequency is measured in units of k_BT. Then $\omega=1$ corresponds to 209 cm^{-1}, again at $T=300$ K. At the carrier concentration of $n_0=3\times10^{17}$ cm^{-1}, the bulk plasma frequency of n-type GaAs is $\omega_p=189$ cm^{-1}, or in our dimensionless units, $\omega_p=0.91k_BT$. For these numbers, the background dielectric constant ϵ is taken to be equal to 10.9, the value of ϵ_∞ in GaAs.

In Fig. 2, for several values of $q_{\parallel}$, we plot $P(q_{\parallel},\omega)$ for n-type GaAs at room temperature ($T=300$ K), with $n_0=3\times10^{17}$ cm^{-3}, and zero surface charge, $Q_s=0$. In the Thomas-Fermi description of the charge profile near the surface,[4] this is the case of zero band bending, though the fully quantum mechanical discussion shows a dipole layer is necessarily present, as a consequence of the boundary condition in Eq. (2.9). Because of this, the value of the self-consistent potential at the surface, measured relative to the bulk is nonzero, so in fact we have band bending by this criterion.

The results in Fig. 2 are typical of those we have obtained in various cases we have examined. They are also similar to those obtained in theoretical studies of surfaces of nearly free electron metals, though here the interesting range of wave vectors $q_{\parallel}$ is the order of 10^6 cm^{-1}, while in the case of metals the relevant scale is 10^8 cm^{-1}. For small $q_{\parallel}$, $P(q_{\parallel},\omega)$ is dominated by a single, prominent surface plasmon resonance close to the surface plasmon frequency $\omega_s=[4\pi n_0e^2/m^*(\epsilon+1)]^{1/2}$ given by dielectric theory. There is appreciable dispersion, even for the smallest value of $q_{\parallel}$ shown in Fig. 2. Thus, for $q_{\parallel}=0.2$, the peak in the loss function lies a bit above $\omega=1$, while in our dimensionless units, $\omega_s=0.87$. As $q_{\parallel}$ increases the peak moves upwards and broadens, to the point where when $q_{\parallel}=0.8$, $P(q_{\parallel},\omega)$ consists of a broad, structureless feature. The broadening has its origin in Landau damping, which is absent from both local dielectric theories[6,7] and hydrodynamics models.[14] This Landau damping occurs because the surface plasmon frequency lies within the particle-hole continuum, so when a surface plasmon is excited, its lifetime is limited because it may create particle-hole pairs.

In Fig. 3, we show $P(q_{\parallel},\omega)$ as a function of Q_s, for $q_{\parallel}=0.4$, and again a carrier concentration of $n_0=3\times10^{17}$ cm^{-3}; recall that Q_s measures the charge deficit in the conduction electrons produced by the presence of charge trapped on the surface. Thus, a negative value of Q_s corresponds to an accumulation layer. The surface plasmon

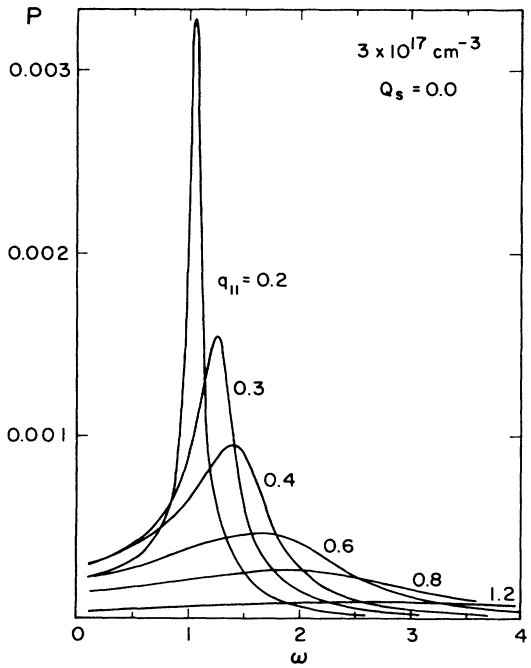

FIG. 2. For the carrier density $n_0=3\times10^{17}$ cm^{-3}, in n-type GaAs at $T=300$ K, we plot the loss function $P(q_{\parallel},\omega)$ for several values of $q_{\parallel}$. The units are the dimensionless units defined in the text.

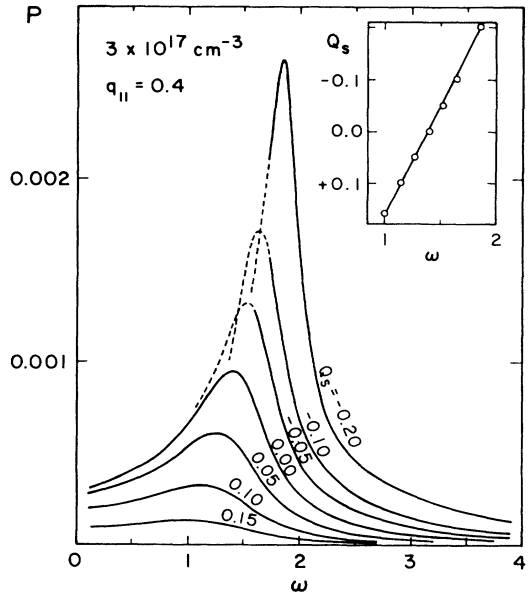

FIG. 3. For $n_0=3\times10^{17}$ cm^{-3}, $T=300$ K and $q_{\parallel}=0.4$, we show the loss function as a function of surface charge Q_s. The inset plots the position of the peak in the loss function, against Q_s. Again, dimensionless units defined in the text are employed.

peak shifts upward with accumulation layer formation, and downward with a depletion layer present. This is as expected on qualitative grounds. The inset in Fig. 3 plots the position of the peak in $P(q_{\parallel},\omega)$, as a function of Q_s. We see a roughly linear dependence. Another striking feature of these results is the variation of the width of the loss structure with Q_s. The surface plasmon loss feature narrows and increases in intensity with formation of an accumulation layer, and is broadened and weakened by the more diffuse depletion layer, acquiring a predominantly single-pair excitation character as discussed below.

The dashed portion of the curves in Fig. 3 correspond to regions where we find rather fine oscillations of the order of $\pm 10\%$ in the calculated loss function. These are strongest at low frequencies, and hence become relatively more prominent at lower carrier concentrations, e.g., 10^{17} cm^{-3}. These oscillations are present in the kernel χ_0, and survive in the full solution χ. Since they occur only for the cases where an accumulation layer is present, they may be real with origin in interband transitions between bound levels produced by the accumulation layer, or between a bound level and the nearby continuum. We find the oscillations only when one or more bound state is present. (Note: These oscillations do not survive when integrating the Green's functions over energies far off the real axis.)

In Figs. 4(a)–4(c), and for three values of Q_s, we plot the variation with $q_{\parallel}$ of the maximum of the loss function. It is evident that as $q_{\parallel}\rightarrow 0$, all frequencies lie near ω_s, as required by Eq. (2.22). The insets show the spatial variation of the free-carrier densities $n(z)$ for each case considered. It is evident that greatest sensitivity to the free-carrier profile occurs when $q_{\parallel} l \sim 1$, with l the thickness of the transition region between the surface and the bulk. As the carrier concentration n_0 increases, l decreases, and the "bulge" in the three sets of curves moves to larger values of $q_{\parallel}$.

For $Q_s=0$, and $n_0=10^{18}$ cm^{-3}, the surface plasmon dispersion curve is quite linear, in its dependence on $q_{\parallel}$, over much of the range explored. A distinct upward curvature appears as the carrier concentration decreases. The origin of this behavior is that the surface plasmon frequency approaches the particle-hole excitation spectrum with increasing $q_{\parallel}$ at the lower concentration, and upward curvature is induced by the resulting coupling. As the intensity of the plasmonlike feature decreases with decreasing electron density or increasing $q_{\parallel}$, it merges into the contribution to the spectrum which is due to single pair excitations.

Notice that rather strong accumulation layers have been explored in Fig. 4. For $n_0=10^{17}$ cm^{-3}, and $Q_s=-0.08$, the maximum charge density in the accumulation layer rises to roughly four times the bulk value. As remarked in Sec. I, for all of our calculations, we find only a single loss peak, with no evidence of contributions from extra branches[6,7] or modes of multipole character,[8] a result we have commented on earlier in this paper. We examined this issue for stronger accumulation layers than illustrated in Fig. 4; for $n_0=10^{18}$ cm^{-3}, we have examined values of Q_s as large as -0.40 (or 2×10^{12} e/cm^2), to always find only a single plasmon peak in the loss function.

So far, we have explored the dynamic response of the surface region for free carriers placed in a semi-infinite dielectric, with dielectric constant ϵ_∞ independent of frequency. In fact, GaAs (and other polar semiconductors) have an infrared active transverse optical phonon at long wavelengths. The background dielectric constant then is frequency dependent, and of the form

$$\epsilon(\omega)=\epsilon_\infty+\frac{\omega_{\mathrm{TO}}^2(\epsilon_0-\epsilon_\infty)}{\omega_{\mathrm{TO}}^2-\omega^2}\ , \tag{4.1}$$

where ω_{TO} is the frequency of the long-wavelength transverse optical phonon, and ϵ_0 the static dielectric constant. Since ω_{TO} and ω_s can be comparable in value, the calculations must be extended to incorporate the dynamic response of the lattice. Within the framework of dielectric theory applied to the semi-infinite medium, surface modes occur when $\epsilon_T(\omega)=-1$, where $\epsilon_T(\omega)=\epsilon(\omega)-\omega_p^2/\omega^2$,

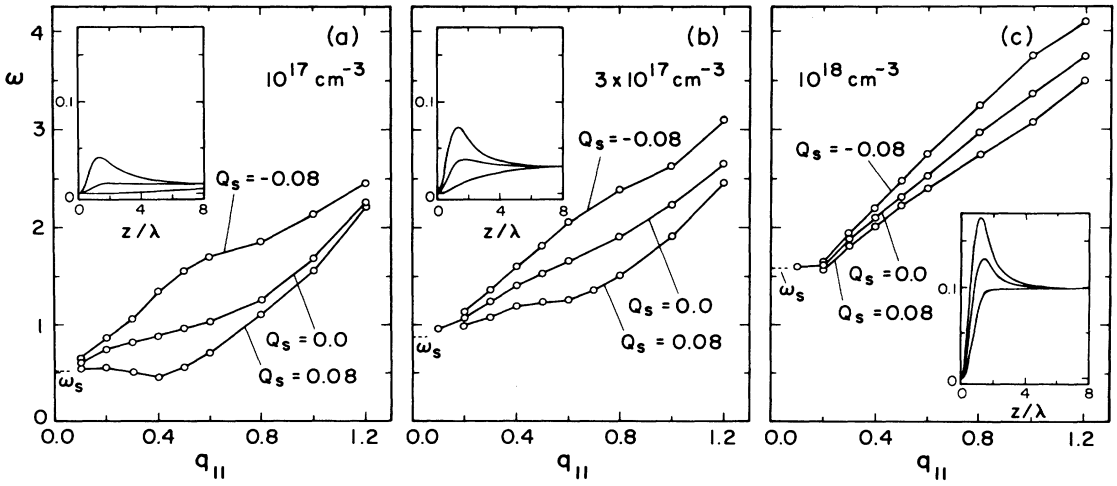

FIG. 4. For $T=300$ K, and a carrier concentration of (a) $n_0=10^{17}$ cm^{-3}, (b) $n_0=3\times10^{17}$ cm^{-3}, and (c) $n_0=10^{18}$ cm^{-3}, we plot the position of the peak in the loss function as a function of $q_{\parallel}$, for the values of the surface charge deficit shown. The insets show the spatial variation of the free-carrier density, for each case considered.

with $\epsilon(\omega)$ given by Eq. (4.1). There are now two roots of the equation $\epsilon_T(\omega)=-1$; each surface mode can be viewed as an admixture of a surface plasmon, with a surface optical phonon (the Fuchs-Kliewer mode). The paper of Matz and Lüth[9] presents calculations of the frequencies of the coupled surface modes, as given by dielectric theory, as a function of carrier concentration, for n-type GaAs.

We may incorporate the lattice response into our calculations of $P(q_\parallel,\omega)$ as follows. First, in the expression for the electron-electron interaction, Eq. (2.19), we use the frequency-dependent form in Eq. (4.1). Also, when we convert the electronic contribution to the loss function, $P_e(q_\parallel,\omega)$ to the full loss function through use of Eq. (2.7), we also use the frequency-dependent dielectric function here as well. This procedure is rigorous in the limit of zero damping of the lattice motion. In our numerical calculations, we added a damping term of the form $-i\omega\Gamma$ into the resonance denominator of Eq. (4.1), choosing $\Gamma=0.1$.

We display results of such calculations in Fig. 5, where for $Q_s=0.0$ and different carrier concentrations, we display the various loss functions. In each figure, the dashed lines show calculations of $P(q_\parallel,\omega)$ which ignore the dynamic response of the lattice by replacing ϵ by ϵ_∞ everywhere. These curves are thus calculated within the framework used for the results shown earlier. The dotted-dashed curve gives $P_e(q_\parallel,\omega)$ calculated with use of full dynamic dielectric constant in Eq. (4.1). So that the result is readily displayed on the same graph as the other functions displayed, we have multiplied $P_e(q_\parallel,\omega)$ by the numerical factor $4/(1+\epsilon_\infty)^2$. Finally, the solid curve in each inset is the full loss function $P(q_\parallel,\omega)$ given in Eq. (2.7), with dynamic screening incorporated also in the prefactor.

The frequency of the Fuchs-Kliewer surface phonon on the surface of undoped GaAs is $\omega_{\rm TO}(1+\epsilon_0)^{1/2}/(1+\epsilon_\infty)^{1/2}$, and this equals 1.40 in the present units. Thus, as one sees from the dashed curves in Fig. 5, the range of free-carrier concentrations explored cover the regime where ω_s lies well below 1.40, to that where it lies well above the Fuchs-Kliewer frequency. When ω_s lies either well below [Fig. 5(a)] or well above [Fig. 5(d)] the Fuchs-Kliewer frequency, the full loss function consists of a doublet, as expected from dielectric theory. In Fig. 5(a), there is a modest upshift of the high-frequency peak to 1.43 produced by the presence of the electron plasma, while in Fig. 5(d), the low frequency feature lies at 1.40. At a concentration where ω_s lies quite close to the Fuchs-Kliewer frequency [Fig. 5(b)], we have a single structure with a highly asymmetric line shape.

Given the response function $\chi(q_\parallel,\omega;z,z')$, we can also analyze the response of the surface region to an externally applied electric field. Suppose the system is driven by an external electric field $\mathbf{E}_{\rm ext}(\mathbf{x},t)$, derivable from an externally applied potential. Let the electric field have frequency ω, spatial variation parallel to the surface given by $\exp(iq_\parallel x)$, and let $E_{\rm ext}(q_\parallel,\omega;z)$ describe the spatial variation of its amplitude with distance from the surface. Such a field sets up charge fluctuations in the material which give rise to an induced electric field $E_{\rm ind}(q_\parallel,\omega;z)$. The induced field is given by

$$E_{\rm ind}(q_\parallel,\omega;z)=-\int_0^\infty dz'\int_0^\infty dz''\,v(q_\parallel;z,z')\chi(q_\parallel,\omega;z',z'')\times E_{\rm ext}(q_\parallel,\omega;z'')\ . \tag{4.2}$$

Here of course the cutoff z_c in the integration has to be chosen larger than when calculating the loss function. To evaluate $E_{\rm ind}$ for $z\le z_m$, we used $z_c=z_m+8/q_\parallel$.

In Fig. 6, we illustrate the response of the system to a field that is independent of z, i.e., the external field has

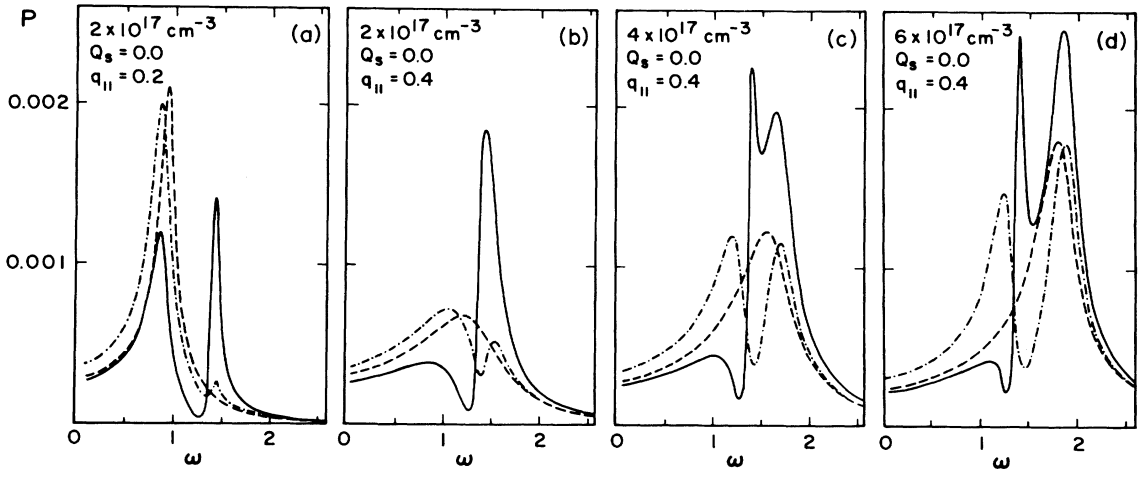

FIG. 5. For $Q_s=0$, and various carrier concentrations, we illustrate the influence of the dynamic response of the lattice on the loss spectrum. In each inset, the dashed line displays $P(q_\parallel,\omega)$ calculated with ϵ replaced by ϵ_∞ everywhere. The dotted-dashed line displays $4/(1+\epsilon_\infty)^2P_e(q_\parallel,\omega)$, with the dynamic response of the lattice incorporated into the calculation of P_e, and the solid line is the full loss function, calculated from Eq. (2.7) with the dynamic response of the lattice used everywhere.

$E_{ext}(q_{\parallel},\omega;z)=E_{ext}(q_{\parallel},\omega)$. The calculations are for an electron density of 10^{18} cm^{-3}, $Q_s=0.0$, and $q_{\parallel}=0.4$, and the figure shows the induced field for several frequencies. There is an exponential tail of the induced field that necessarily extends into the vacuum, as a consequence of the fact that the induced potential ϕ_{ind} must satisfy Laplaces equation in the vacuum outside the material. We see the induced field rises quickly to a constant value inside the material, as expected from elementary considerations. One notes, however, an appreciable spatial variation for the two frequencies $\omega=2.1$ and $\omega=2.2$. These lie just above ω_s and very close to the bulk plasma resonance, and the resonant response of the free carriers is suppressed near the surface by the reduced electron density there. Thus, one must penetrate into the material some distance before the proper bulk behavior is realized, at such a frequency. In these calculations, the phase of the induced field exhibits little dependence on z, at all frequencies explored. The frequency variation of the phase of the induced field at the surface $z=0$ is illustrated in the inset. Below the plasma resonance, the induced field is 180° out of phase with the external field, as one would expect from dielectric theory. As one passes through the plasma resonance, we see a 180° phase shift so above the resonance, the induced field is in phase with the externally applied field.

In Fig. 7, we show the induced field in response to an external field with spatial variation in the z direction proportional to $\exp(-q_{\parallel}z)$. For two frequencies, we show the real and imaginary part of the field. We see that for $\omega=1.8$, below the bulk plasmon resonance, both the real and imaginary part decay monotonically, beyond the inhomogeneous surface layers. The inset shows the dependence of the complex phase of the induced field with z for such an external field, for several frequencies. For $\omega=1.8$, one sees the phase is almost independent of z. For frequencies above the plasma frequency, such as $\omega=2.4$, we see an oscillatory response. In the medium, the phase now varies *linearly* with z, as indicated in the inset. Quite clearly, the external field has launched a bulk plasma wave, with a wave vector that increases with frequency, as one moves above the bulk plasma frequency. Only the *magnitude* of the induced field decays monotonically with z, for frequencies above the bulk plasma frequency, incidentally. The bulk plasma wave experiences appreciable Landau damping, so the attenuation length is rather short.

In a recent paper, Stahl[21] has presented a microscopic study of surface plasmons, for parameters appropriate to GaAs. His study employs the infinite barrier model, for which the free-carrier density profile is not generated by wave functions derived from a self-consistent potential. Stahl also presents calculations of the response of his model system to an externally applied field with exponen-

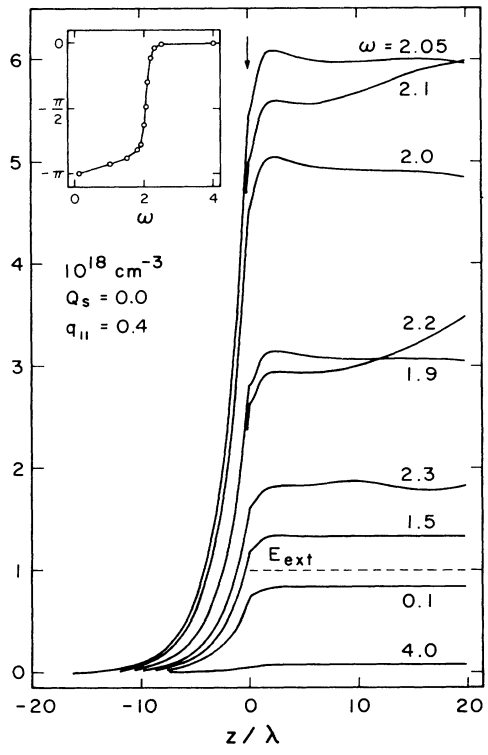

FIG. 6. We show the magnitude and spatial variation of the induced field which appears in response to an externally applied field with the spatial variation $\exp(iq_{\parallel}x)$, independent of z. The external field has amplitude unity, as indicated. The calculations are for a carrier concentration of 10^{18} cm^{-3} and $Q_s=0.0$, and we have set $q_{\parallel}=0.4$. The inset shows the phase of the induced field, relative to the external field, at the surface.

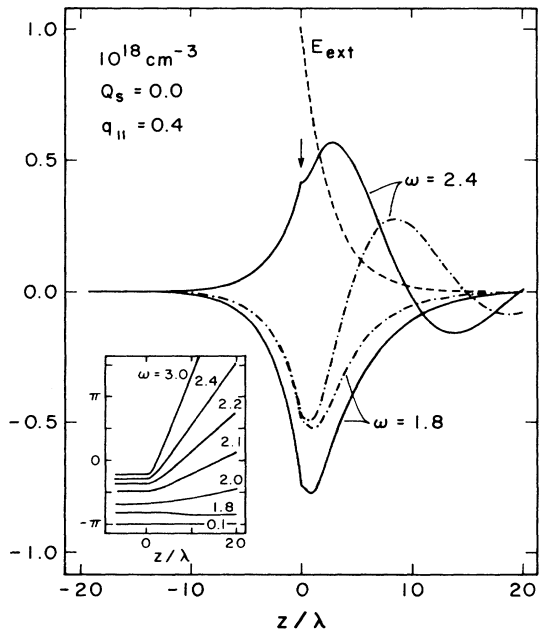

FIG. 7. The real (solid line) and imaginary part (dot-dashed line) of the induced field for $\omega=1.8$ and $\omega=2.4$, in response to an external field with the spatial variation $\exp(iq_{\parallel}x-q_{\parallel}z)$. As in Fig. 6, the free-carrier concentration is 10^{18} cm^{-3}, $Q_s=0.0$ and we have $q_{\parallel}=0.4$. The inset shows the variation of the phase of the induced disturbance, with distance from the surface.

tial profile, and finds results qualitatively similar to those displayed in Fig. 7.

As remarked earlier, these calculations were motivated by the experimental studies of Matz and Lüth, who observed shifts in the surface plasmon frequencies of n-type GaAs, in response to chemisorption of hydrogen on the surface. Unfortunately, we are unable to offer a quantitative interpretation of their data, at this time. In the experiment, as is standard in near-specular electron-energy-loss studies of dipole losses,[3] the angular variation of the near-specular dipole loss feature is not resolved. All electrons which emerge from the crystal within roughly one degree of the specular direction are collected; hence the loss spectrum is an average over a range of wave vectors, as we see in Eq. (2.1), with $0 < q_{\parallel} < 10^6$ cm^{-1} the relevant range. Our calculations show that there is appreciable dispersion of the surface plasmon loss feature in this range of wave vectors, and also that shifts in the loss peak produced by a change in the free carrier profile depend strongly on wave vector (see Fig. 4). It is thus difficult to interpret, in quantitative terms, the shift of a structure in the loss spectrum from a feature that is an average over such a range of wave vectors, in view of these results.

We can make some qualitative remarks. The calculations show that the surface plasmon is rather heavily Landau damped in this wave-vector regime, and we also see the broad particle-hole spectrum prominently in our calculations of the loss function $P(q_{\parallel},\omega)$. If Matz and Lüth's data on doped GaAs is compared with their data on the insulating form of the material, we note that for the insulating material the Fuchs-Kliewer mode stands out clearly as a resolved line, well outside the quasielastic peak. In the loss spectra taken on the n-type material, the loss peaks appear instead as shoulders on a broad background evidently produced by scattering from particle-hole pairs. The combined effects of dispersion and Landau damping such as one sees in our calculation evidently are responsible for the degradation in the prominence of the loss peaks found for the doped material.

We also note that Matz and Lüth also examined only the case where the adsorbates induced a depletion layer. We have seen that (Fig. 3) as a depletion layer is formed, the surface plasmon resonance is broadened and, as expected from the f-sum rule, weakened. These are in fact trends evident in other calculations we have performed which are not displayed in this paper. It would be of considerable interest to see experiments on surfaces where an accumulation layer is present. We see, again from Fig. 3, that in this case the surface plasmon feature sharpens and increases in intensity. Thus, the surface charge induced shift in the surface plasmon frequency should be easier to observe quantitatively.

In our view, it would be of very great interest to see angle resolved studies of the near-specular dipole lobe in systems such as that explored here. This would provide direct experimental access to both the dispersion and Landau damping of surface plasmons found in our calculations, and through modulation of the free carrier profile by chemisorption one could also examine the dependence of the line shapes and frequencies on the free-carrier density profile. In principle, such angle resolved studies of the near-specular dipole peak could provide unique and detailed data on the dynamic response of the nonuniform electron gas; we know of no other spectroscopy which has the potential of exploring the inhomogeneous electron gas in precisely the range $q_{\parallel} l \sim 1$, with l the spatial scale of the nonuniformity in density. In addition to addressing the basic question just described, such spectroscopic studies would be of great interest as a probe of free carriers near the surface of technologically important semiconducting materials.

Very clearly, angle-resolved studies of the near-specular lobe cannot be carried out by minor modifications of existing electron-energy-loss spectrometers. However, the intensity in the dipole lobe is substantial. It would be of great interest to explore the feasibility of designing a system which could achieve high resolution in wave vector near the specular, possibly achieved by sacrificing intensity. Clearly, pursuit of this question is beyond the scope of the present authors.

It is not necessary to have full angle-resolved capability to obtain information on wave-vector-dependent features in energy-loss spectra such as studied here. In their study of surface plasmons on the surface of InSb, with depletion layer present, Ritz and Lüth[10] have explored the position and width of the surface-plasmon-loss structure as a function of primary beam energy. As the beam energy is decreased, the surface-plasmon-loss structure shifts to higher frequency, broadens substantially, and decreases in intensity. These authors argue that the average wave vector of the surface plasmons sampled in the experiment varies inversely with the square root of the beam energy, a result which follows from the general structure of the dipole-loss cross section. Thus, with decreasing beam energy, they sample surface plasmons with increasing wave vector; the sequence of loss spectra in their Fig. 1 bear a striking qualitative resemblance to the calculations displayed in Fig. 2 of the present paper. It remains true, however, that each of their loss spectra remains an average of a range of surface plasmon wave vectors, so quantitative comparison with calculations of $P(q_{\parallel},\omega)$ cannot be made. Of course, the experiments also explore InSb, and not GaAs. Straightforward application of our calculation to InSb is also not possible, since for the carrier concentrations explored, deviations from parabolicity are important in the conduction band.

ACKNOWLEDGMENTS

This research was supported by the U.S. Department of Energy, through Grant No. DE-FG03-84ER45083. One of us (D.H.E.) wishes also to acknowledge financial support from the German Academic Exchange Service [Deutscher Akademischer Austauschdienst (DAAD)].

APPENDIX: THE BEHAVIOR OF THE RESPONSE FUNCTION AT FINITE FREQUENCY, IN THE LIMIT $\mathbf{q}_{\parallel}=\mathbf{0}$

We begin by noting that the single-particle eigenstates in Eq. (2.16) are always real, so we may begin by studying

$$\chi_0(\mathbf{q}_\parallel,\omega;z,z')=\frac{2}{A}\sum_{\mathbf{k}_\parallel}\sum_{i,j}\frac{[f(\mathbf{k}_\parallel,i)-f(\mathbf{k}_\parallel+\mathbf{q}_\parallel,j)]}{(\hbar\omega+E_{\mathbf{k}_\parallel+\mathbf{q}_\parallel,j}-E_{\mathbf{k}_\parallel i})}\psi_i(z)\psi_i(z')\psi_j(z)\psi_j(z')\ , \tag{A1}$$

which may be rearranged to read

$$\chi_0(\mathbf{q}_\parallel,\omega;z,z')=\frac{2}{\hbar\omega A}\sum_{\mathbf{k}_\parallel}\sum_{i,j}\psi_i(z)\psi_j(z)\psi_i(z')\psi_j(z')f(\mathbf{k}_\parallel,i)\left[\frac{1}{1-\frac{1}{\hbar\omega}(E_{\mathbf{k}_\parallel,i}-E_{\mathbf{k}_\parallel+\mathbf{q}_\parallel,j})}-\frac{1}{1+\frac{1}{\hbar\omega}(E_{\mathbf{k}_\parallel,i}-E_{\mathbf{k}_\parallel+\mathbf{q}_\parallel,j})}\right]. \tag{A2}$$

We assume the frequency is sufficiently large that we may expand in inverse powers of ω. We do this, and retain only the leading term, so

$$\chi_0(\mathbf{q}_\parallel,\omega;z,z')=\frac{4}{\hbar^2\omega^2 A}\sum_{i,j}\sum_{\mathbf{k}_\parallel}\psi_i(z)\psi_j(z)\psi_i(z')\psi_j(z')f(\mathbf{k}_\parallel,i)(E_{\mathbf{k}_\parallel,i}-E_{\mathbf{k}_\parallel+\mathbf{q}_\parallel,j})\ . \tag{A3}$$

Note that the validity of the step just taken is not insured by the assumption that $\mathbf{q}_\parallel$ is small. This suffices for the intraband contributions with $j=i$, but not for those from the "interband" virtual transitions. We require both that $\mathbf{q}_\parallel$ be small (so the expansion is valid for intraband terms), and also that ω be large compared to the energy of the interband contributions.

On physical grounds, the second condition is required because surface plasmons are Landau damped even at $\mathbf{q}_\parallel\equiv 0$ by virtue of the breakdown of momentum conservation normal to the surface. Only when ω is large compared to the interband transitions may Landau damping be set aside in the surface problem, and then an expansion such as that in Eq. (A3) may be used.

To proceed, recall $E_{\mathbf{k}_\parallel,i}=\varepsilon_i+\hbar^2k_\parallel^2/2m^*$. Then for small $\mathbf{q}_\parallel$, Eq. (A3) may be replaced by

$$\chi_0(\mathbf{q}_\parallel,\omega;z,z')\cong\frac{4}{\hbar^2\omega^2 A}\sum_{i,j}\sum_{\mathbf{k}_\parallel}\psi_i(z)\psi_j(z)\psi_i(z')\psi_j(z')f(\mathbf{k}_\parallel,i)(\varepsilon_i-\varepsilon_j)\ , \tag{A4}$$

or

$$\chi_0(\mathbf{q}_\parallel,\omega;z,z')=\frac{2}{\hbar^2\omega^2}\sum_{i,j}n_i\psi_i(z)\psi_j(z)\psi_i(z')\psi_j(z')(\varepsilon_i-\varepsilon_j) \tag{A5}$$

where

$$n_i=\frac{2}{A}\sum_{\mathbf{k}_\parallel}f(\mathbf{k}_\parallel,i)\ , \tag{A6}$$

the number of electrons in subband i.

Now the single-particle wave functions obey the Schrödinger equation

$$-\frac{\hbar^2}{2m^*}\frac{d^2\psi_i}{dz^2}+V(z)\psi_i=\varepsilon_i\psi_i \tag{A7}$$

with $V(z)$ the self-consistent potential, and one then derives the identity

$$(\varepsilon_j-\varepsilon_i)\psi_i(z)\psi_j(z)=\frac{\hbar^2}{2m^*}\frac{d}{dz}\left[\psi_j\frac{d\psi_i}{dz}-\psi_i\frac{d\psi_j}{dz}\right]. \tag{A8}$$

Hence in the limit of interest, we have

$$\chi_0(\mathbf{0},\omega;z,z')=-\frac{1}{m^*\omega^2}\sum_{i,j}n_i\psi_i(z)\psi_j(z)\times\frac{d}{dz'}\left[\psi_j(z')\frac{d\psi_i}{dz'}-\psi_i(z')\frac{d\psi_j}{dz'}\right]. \tag{A9}$$

We now turn to the equation satisfied by the full response function $\chi(\mathbf{q}_\parallel,\omega;z,z')$. For the purposes of the issue at hand, it will be useful to generalize Eq. (2.15) to include also the effective short-ranged electron-electron couplings generated by exchange and correlation. If we introduce exchange and correlation into Eq. (2.15), of course, self-consistency requires its influence be incorporated into the self-consistent potential which generates the single particle states $\psi_i(z)$,[11] though we need not take explicit account of this at present. Thus, we extend Eq. (2.15) to read, replacing $\chi_0(\mathbf{q}_\parallel,\omega;z,z')$ by $\chi_0(\mathbf{0},\omega;z,z')$ for present purposes,

$$\chi(\mathbf{q}_\parallel,\omega;z,z')=\chi_0(\mathbf{q}_\parallel,\omega;z,z')-\int_0^\infty dz''\int_0^\infty dz'''\,\chi_0(\mathbf{0},\omega;z,z'')v(q_\parallel;z'',z''')\chi(\mathbf{q}_\parallel,\omega;z''',z')$$
$$-\int_0^\infty dz''\,\chi_0(\mathbf{0},\omega;z,z'')v_{xc}(z'')\chi(q_\parallel,\omega;z'',z')\ . \tag{A10}$$

In the χ_0 which appears in the inhomogeneous term, it is important to retain $\mathbf{q}_\parallel$ as finite, though our interest is in the case $\mathbf{q}_\parallel$ very small.

Call the exchange-correlation term on the right-hand side of Eq. (A10) $\Gamma_{xc}(zz')$. With Eq. (A9) inserted,

$$\Gamma_{\rm xc}(z,z')=+\frac{1}{m^*\omega^2}\sum_{i,j} n_i\psi_i(z)\psi_j(z)\int_0^\infty dz''\frac{d}{dz''}\left[\psi_j(z'')\frac{d\psi_i}{dz''}-\psi_i(z'')\frac{d\psi_j}{dz''}\right]v_{\rm xc}(z'')\chi(q_\parallel,\omega;z'',z') \ . \tag{A11}$$

A partial integration gives

$$\Gamma_{\rm xc}(zz'')=-\frac{1}{m^*\omega^2}\sum_{i,j} n_i\psi_i(z)\psi_j(z)\int_0^\infty dz''\left[\psi_j(z'')\frac{d\psi_i}{dz''}-\psi_i(z'')\frac{d\psi_j}{dz''}\right]\frac{d}{dz''}[v_{\rm xc}(z'')\chi(q_\parallel,\omega;z'',z')] \ , \tag{A12}$$

where the boundary terms vanish by virtue of the condition in Eq. (2.12), and the fact that for finite z', $\lim_{z''\to\infty}\chi(q_\parallel\omega;z'',z')=0$. A second partial integration on the term proportional to $\psi_i(d\psi_j/dz'')$ gives

$$\begin{aligned}\Gamma_{\rm xc}(zz')=&-\frac{2}{m^*\omega^2}\sum_{i,j} n_i\psi_i(z)\psi_j(z)\int_0^\infty dz''\,\psi_j(z'')\frac{d\psi_i}{dz''}\frac{d}{dz''}[v_{\rm xc}(z'')\chi(q_\parallel,\omega;z'',z')]\\&-\frac{1}{m^*\omega^2}\sum_{i,j} n_i\psi_i(z)\psi_j(z)\int_0^\infty dz''\,\psi_i(z'')\psi_j(z'')\frac{d^2}{(dz'')^2}[v_{\rm xc}(z'')\chi(q_\parallel,\omega;z'',z')] \ .\end{aligned} \tag{A13a}$$

We may now invoke the completeness relation

$$\sum_j \psi_j(z)\psi_j(z'')=\delta(z-z'') \tag{A13b}$$

and note $n(z)=\sum_i n_i\psi_i^2(z)$ is the electron density at point z. We then have, as $q_\parallel\to 0$ with ω finite,

$$\Gamma_{\rm xc}(z,z')=-\frac{1}{m^*\omega^2}\frac{d}{dz}\left[n(z)\frac{d}{dz}v_{\rm xc}(z)\chi(q_\parallel,\omega;z,z')\right] \ . \tag{A14}$$

We now turn to the direct Coulomb term, and consider the combination

$$\Gamma_c(z,z')=\int_0^\infty dz''\,\chi_0(\mathbf{0},\omega;z,z'')v(q_\parallel;z'',z') \ , \tag{A15}$$

which becomes, after use of Eq. (A9) and a partial integration,

$$\Gamma_c(z,z')=\frac{1}{m^*\omega^2}\sum_{i,j} n_i\psi_i(z)\psi_j(z)\int_0^\infty dz''\left[\psi_j(z'')\frac{d\psi_i}{dz''}-\psi_i(z'')\frac{d\psi_j}{dz''}\right]\frac{dv(q_\parallel;z'',z')}{dz''} \ . \tag{A16}$$

As $\mathbf{q}_\parallel\to\mathbf{0}$, we have from Eq. (2.19) of the text

$$\lim_{q_\parallel\to 0}\frac{dv(q_\parallel;z'',z')}{dz''}=\frac{4\pi e^2}{\epsilon+1}\left[\frac{1}{\epsilon}\Theta(z'-z'')-\Theta(z''-z')\right] \ . \tag{A17}$$

When this is employed in Eq. (A16), after a partial integration we find

$$\begin{aligned}\Gamma_c(z,z')=&-\frac{4\pi e^2}{m^*\omega^2(\epsilon+1)}\sum_i n_i\psi_i(z)\left[\left[\frac{\epsilon+1}{\epsilon}\right]\psi_i(z')\left[\sum_j\psi_j(z)\psi_j(z')\right]+2\int_{z'}^\infty dz''\left[\sum_j\psi_j(z)\psi_j(z'')\right]\frac{d\psi_i}{dz''}\right.\\&\left.-\frac{2}{\epsilon}\int_0^{z'}dz''\left[\sum_j\psi_j(z)\psi_j(z'')\right]\frac{d\psi_i}{dz''}\right] \ .\end{aligned} \tag{A18}$$

After use of the completeness relation in Eq. (A13b), Eq. (A18) may be reduced to

$$\Gamma_c(z,z')=-\frac{4\pi n(z)e^2}{\epsilon m^*\omega^2}\delta(z-z')-\frac{4\pi e^2}{m^*(\epsilon+1)\omega^2}\frac{dn}{dz}\left[\Theta(z-z')-\frac{1}{\epsilon}\Theta(z'-z)\right] \ . \tag{A19}$$

When Eq. (A19) and Eq. (A14) are introduced in Eq. (A10), as $q_\parallel\to 0$ with ω finite, Eq. (A10) is replaced by

$$\begin{aligned}\chi(q_\parallel,\omega;z,z')=&\chi_0(q_\parallel,\omega;z,z')+\frac{4\pi n(z)e^2}{\epsilon m^*\omega^2}\chi(q_\parallel,\omega;z,z')\\&+\frac{4\pi e^2}{(\epsilon+1)m^*\omega^2}\frac{dn}{dz}\left[\int_0^z dz''\chi(q_\parallel,\omega;z'',z')-\frac{1}{\epsilon}\int_z^\infty dz''\chi(q_\parallel,\omega;z'',z')\right]\\&+\frac{1}{m^*\omega^2}\frac{d}{dz}\left[n(z)\frac{d}{dz}v_{\rm xc}(z)\chi(q_\parallel,\omega;z,z')\right] \ .\end{aligned} \tag{A20}$$

Further partial integrations and rearrangement leads us to rewrite Eq. (A20) as

$$\chi(q_\parallel,\omega;z,z')=\chi_0(q_\parallel,\omega;z,z')-\frac{4\pi e^2}{\epsilon m^*\omega^2}\frac{d}{dz}\left[n(z)\int_z^\infty dz''\,\chi(q_\parallel,\omega;z'',z')\right]$$
$$+\frac{4\pi e^2}{m^*(\epsilon+1)}\left[\frac{dn}{dz}\right]\int_0^\infty dz''\chi(q_\parallel,\omega;z'',z')+\frac{1}{m^*\hbar^2\omega^2}\frac{d}{dz}\left[n(z)\frac{d}{dz}v_{xc}(z)\chi(q_\parallel,\omega;z,z')\right]. \tag{A21}$$

We now integrate both sides of Eq. (A21) from $z=0$ to $z=\infty$. The boundary conditions in Eq. (2.12) of the text requires $n(z)$ to vanish at $z=0$. This again combined with the fact that $\lim_{z\to\infty}\chi(q_\parallel,\omega;z,z')=0$ with z' fixed means that the exchange term drops out, after this integration. We then find

$$\int_0^\infty dz\,\chi(q_\parallel,\omega;z,z')=\int_0^\infty dz\,\chi_0(q_\parallel,\omega;z,z')+\frac{4\pi n(\infty)e^2}{m^*(\epsilon+1)}\frac{1}{\omega^2}\int_0^\infty dz\,\chi(q_\parallel,\omega;z,z')\,. \tag{A22}$$

Throughout the discussion except in certain sensitive places (the inhomogeneous term, for example), we have let $q_\parallel\to 0$, so where $q_\parallel$ appears it is to be viewed as very small. For such small values of $q_\parallel$, and z' fixed near the surface, there is no difference between $\int_0^\infty dz\,\chi(q_\parallel,\omega;z,z')$, and $\int_0^\infty dz\,\chi(q_\parallel,\omega;z,z')\exp(-q_\parallel z)$. Thus, we have established the following identity, from the RPA equation supplemented by exchange and correlation corrections:

$$\lim_{q_\parallel\to 0}\int_0^\infty dz\,\chi(q_\parallel,\omega;z,z')\exp(-q_\parallel z)=\frac{\lim_{q_\parallel\to 0}\left[\int_0^\infty dz\,\chi_0(q_\parallel,\omega;z,z')\right]}{1-[4\pi n(\infty)e^2/m^*(\epsilon+1)\omega^2]}\,. \tag{A23}$$

Finally, consider the numerator in Eq. (A23). In the high-frequency limit, Eq. (A3) gives

$$\int_0^\infty dz\,\chi_0(q_\parallel,\omega;z,z')=\frac{4}{\hbar^2\omega^2 A}\sum_{\mathbf{k}_\parallel i}f(\mathbf{k}_\parallel,i)\psi_i^2(z')(E_{\mathbf{k}_\parallel,i}-E_{\mathbf{k}_\parallel+\mathbf{q}_\parallel,i})\equiv-\frac{q_\parallel^2 n(z')}{m^*\omega^2} \tag{A24}$$

Hence we have established the following identity:

$$\lim_{q_\parallel\to 0}\int_0^\infty dz\,\chi(q_\parallel,\omega;z,z')e^{-q_\parallel z}=\frac{-q_\parallel^2}{m^*\omega^2}\frac{n(z')}{1-[4\pi n(\infty)e^2/m^*(\epsilon+1)]\frac{1}{\omega^2}}\,. \tag{A25}$$

The right-hand side has a pole at the frequency ω_s that is the frequency of the surface plasmon of dielectric theory. The frequency is

$$\omega_s=\left[\frac{4\pi n(\infty)e^2}{m^*(\epsilon+1)}\right]^{1/2}, \tag{A26}$$

unaffected by details of the surface profile, or the presence of exchange and correlation.

To obtain the result displayed in Eq. (A25), the reader will appreciate that inclusion of the image-charge contribution to the electron-electron interaction is essential.

*Present address: Max-Planck-Institut für Festkörperforschung, Heisenbergstrasse 1, D-7000 Stuttgart 80, Federal Republic of Germany.

[1]See Sec. X of E. Burstein and D. L. Mills, Rep. Prog. Phys. **37**, 817 (1974).

[2]Throughout this paper, we confine our attention to n-type semiconductors, with electrons of effective mass m^* in a parabolic conduction band.

[3]See H. Ibach and D. L. Mills, the discussion in Chap. 3 of *Electron Energy Loss Spectroscopy and Surface Vibrations* (Academic, San Francisco, 1982).

[4]See, for example, J. P. McKelvey, the discussion which begins on page 489 of *Solid State and Semiconductor Physics* (Harper and Row, New York, 1966).

[5]D. H. Ehlers and D. L. Mills, Phys. Rev. B **34**, 3939 (1986).

[6]S. L. Cunningham, A. A. Maradudin, and R. F. Wallis, Phys. Rev. B **10**, 3342 (1974).

[7]In the literature on surface plasmons in the presence of nonuniform free-carrier density profiles, considerable controversy arose over the question of the number of branches present, over and above the single branch provided by the macroscopic theory of the semi-infinite dielectric. See E. M. Conwell, Solid State Commun. **14**, 915 (1974); Phys. Rev. B **11**, 1510 (1975); C. C. Kao and Esther Conwell, *ibid.* **14**, 2464 (1976). Distinctly different results for the same model were found by D. Guidotti, S. A. Rice, and H. L. Lemberg, Solid State Commun. **15**, 113 (1974); S. A. Rice, D. Guidotti, H. L. Lemberg, W. C. Murphy, and A. N. Block, in *Advances in Chemical Physics,* edited by I. Prigogine and S. A. Rice (Wiley, New York, 1974), Vol. XXVII. See also E. M. Conwell, Phys. Rev. B **14**, 5515 (1976) for criticism of the method used by Guidotti *et al.*; D. Guidotti and S. A. Rice, *ibid.* **14**, 5518 (1976).

[8]For n-type GaAs at room temperature, the de Broglie wave-

length of an electron with energy $\frac{3}{2}k_BT$ is 237 Å, and the Debye screening length is 136 Å if the carrier density is 10^{17} cm^{-3}.

[9]R. Matz and H. Lüth, Phys. Rev. Lett. **46**, 500 (1981).

[10]A. Ritz and H. Lüth, Phys. Rev. Lett. **52**, 1242 (1984).

[11]A. Liebsch, Phys. Rev. Lett. **54**, 67 (1985).

[12]D. L. Mills, Surf. Sci. **48**, 59 (1975).

[13]This singular behavior is illustrated in Fig. 3 of Ref. 6.

[14]In the limit $q_{\parallel}\rightarrow 0$, where $q_{\parallel}$ is the wave vector of the surface plasmon, a proof given later in this text shows that (with retardation ignored) there is only one surface mode which contributes to the loss function probed in an electron-energy-loss experiment, independently of the nature of the carrier density profile. The frequency of this mode is $\omega_p/(1+\epsilon)^{1/2}$, as given by macroscopic dielectric theory. All other modes, such as the high-frequency multipole modes found in hydrodynamic theory must, if they survive in a full theory have oscillator strength which vanishes as $q_{\parallel}\rightarrow 0$. Multipole modes in hydrodynamic theory have been discused by A. Eguiluz and J. J. Quinn, Phys. Rev. B **14**, 1347 (1976).

[15]See Eq. (3.9) of Ref. 3, and use Eq. (29a) of E. Evans and D. L. Mills, Phys. Rev. B **5**, 4126 (1972), to cast the result in this form. When, as at present, $P(\mathbf{q}_{\parallel},\omega)$ depends on only $|\mathbf{q}_{\parallel}|$, the angular integration in Eq. (2.1) may be performed in closed form. The result is found in R. E. Camley and D. L. Mills, Phys. Rev. B **29**, 1695 (1984).

[16]G. A. Baraff and J. Appelbaum, Phys. Rev. B **5**, 475 (1972).

[17]A. Zangwill and P. Soven, Phys. Rev. A **21**, 1561 (1980).

[18]For a review of early work see Peter J. Feibelman, Prog. Surf. Sci. **12**, 287 (1982).

[19]A. Eguiluz and D. Campbell, Phys. Rev. B **31**, 7572 (1985).

[20]A. Griffin and J. Harris, Can. J. Phys. **54**, 1396 (1976).

[21]A. Stahl, Surf. Sci. **134**, 297 (1983).